One-pot synthesis of stable $CsPbBr_3$@$CsPb_2Br_5$ core-shell heteronanocrystals with controlled permeability to halide ions

Ignacio Rosa-Pardo,[1] Alessandro Ciccone,[1] Raúl Arenal,[2,3,4] Raquel E. Galian[1] and Julia Pérez-Prieto*[1]*

[1] Photochemistry Reactivity Group (PRG), Institute of Molecular Science, University of Valencia, c/ Cat. José Beltrán 2, Paterna, 46980, Valencia, Spain.

[2] Laboratorio de Microscopias Avanzadas (LMA), Universidad de Zaragoza, Mariano Esquillor s/n, 50018 Zaragoza, Spain.

[3] Instituto de Nanociencia y Materiales de Aragón (INMA), CSIC-U. Zaragoza, Pedro Cerbuna 12, 50009 Zaragoza, Spain.

[4] ARAID Foundation, 50018 Zaragoza, Spain.

AUTHOR INFORMATION

Corresponding Author

*raquel.galian@uv.es, *julia.perez@uv.es

ABSTRACT

A simple one-pot synthetic strategy based on the hot injection methodology was adapted to prepare (photo)stable and green emissive colloidal $CsPbBr_3$@$CsPb_2Br_5$ core@shell heteronanocrystals (HNCs). The photoactive core, specifically $CsPbBr_3$ ternary metal halide nanocrystals, was homogeneously covered with an ultrathin $CsPb_2Br_5$ shell (ca. 2 nm) which confers them with a long-term stability and higher photoluminescence quantum yield. Astonishingly, this heterostructure enabled controlled halide exchange to yield unprecedented $CsPbCl_3$@$CsPb_2Cl_5$ and $CsPbI_3$@$CsPb_2I_5$ heteronanocrystals.

INTRODUCTION

Metal halide perovskite nanocrystals (MHP NCs) have emerged as great candidates for optoelectronic and photovoltaic applications and more recently for photocatalytic applications due to their amazing optical and electronic properties.[1] However, their low stability towards external factors such as light, humidity, and heat hampers their real applications. Several attempts to overcome these limitations include the development of heterostructures.[2] The combination of two or more materials into the nanoscale regime gives rise to new heteronanocrystals (HNCs) with superior properties to the pristine material.[3-4] In this regard, MHP NCs have been combined with metal oxides, metal halides, metal sulfides, and metal ions to produce heterostructures, such as core@shell heterodimers and nanocomposites.[5] Inspired by the knowledge of chalcogenide semiconductor NCs, the growth of a shell on the surface of core NCs to produce core@shell HNCs is a good alternative to overcome the poor stability of MHP NCs against environmental stress. Some criteria must be met to design a core/shell structure, such as i) the selection of a suitable shell material, ii) an adequate band gap alignment between the core and the shell, iii) a small lattice mismatch, and iv) the crystallization of both materials with a similar crystal structure.[6] In this sense, there are multiple organic materials (e.g. phenylpropylammonium bromide and polymethyl methacrylate) and inorganic materials (such as NaBr, TiO_2, and metal chalcogenides, as well as perovskites; e.g. Cs_4PbBr_6, $CsPb_2Br_5$, Rb_4PbBr_6) used for covering a perovskite core.[7-13] The most promising strategy is to cover a perovskite NC with another crystalline perovskite shell to develop a perovskite/perovskite core@shell HNCs that offers a minimal mismatch between the core and the shell. The 2D $CsPb_2Br_5$ perovskite material has been considered a good candidate as coating material due to its indirect band gap (2.979 eV),[14] photoluminescence inactivity, water-resistance properties, and minimal lattice mismatch with $CsPbBr_3$ NCs.

There are several reported strategies for preparing heterostructures or assemblies, which are based on $CsPbBr_3$ and $CsPb_2Br_5$ perovskites, such as the post-synthetic treatment of $CsPbBr_3$ NCs with water[2] and a modified hot injection methodology which uses an excess of $PbBr_2$,[15] low temperature[16] and long reaction time.[3-4, 14]

Although there are several methods to produce metal halide nanocrystals with high emission and homogeneous shape, [17-19] the hot injection methodology has been established as the optimal procedure to provide high-quality monodispersed nanocrystals. In this strategy, the cesium precursor is injected into a high-temperature solution of metal-ligands complexes to bring $CsPbX_3$ (X= Cl^-, Br^-, I^-) nanoparticles.[20] Sheldon et. al. have reported that the growth of $CsPbBr_3$ perovskite NCs starts with the complexation of bromide and cesium to produce CsBr seeds, which react with lead and bromide to generate Cs_4PbBr_6 intermediate that eventually evolves to $CsPbBr_3$. The complexation of bromide anion to cesium cation proved to be the crucial step; additionally, the crystal phase of the products is determined by the bromide concentration. This was demonstrated by slowing the reaction kinetics, specifically by selecting 1-bromohexane as precursor and extending the reaction from a few seconds to 20 minutes.[21]

In the conventional synthesis of $CsPbBr_3$ perovskite NCs, the Cs precursor is preheated at temperatures between 65ºC-100ºC to ensure the formation of Cs-oleate, and then it is usually injected at a temperature higher than 150°C, thereby producing the cubic or orthorhombic perovskite phase.[22-23] However, Sun et al. have demonstrated the formation of the dual phase $CsPbBr_3$-$CsPb_2Br_5$ composite when the reaction was performed at a lower temperature (100°C) and the crystallization occurred at 130°C.[16] An excess of $PbBr_2$ seems to facilitate the generation of the $CsPb_2Br_5$ secondary phase, coming from the structural transformation of $CsPbBr_3$ at low temperatures. The presence of $CsPb_2Br_5$ nanoparticles on the $CsPbBr_3$ NC structure in the composite did not only enhance the current efficiency but it also i) reduced the

trap density in the bang gap, ii) increased the ionic conductivity, and iii) improved the photoluminescence lifetime of the $CsPbBr_3$ NCs.

Furthermore, Rodová et al. have reported the presence of $CsPb_2Br_5$ phase as an impurity of the $CsPbBr_3$ ternary metal halide NCs prepared at 70°C,[24] but it occurred in only a 10 % when the reaction was performed at room temperature.[25] Interestingly, tetragonal $CsPb_2Br_5$ 2D material was obtained after 2 h of reaction at 160°C in the presence of an excess of $PbBr_2$. The crystal structure evolution hypothetically took place via the breaking of the $PbBr_6$ octahedra connection, forming an expanded interlayer, followed by rearrangement of the octahedrons in the a-b axis plane and, as a consequence, the polyhedrons changed to $PbBr_8$ capped triangular prisms.[14]

Bo Qiao et al. have reported on a $CsPbBr_3/CsPb_2Br_5$ core-shell-like structure obtained by a modified non-stoichiometric solution-phase methodology to enhance the water stability of the emissive $CsPbBr_3$.[15] The presence of both crystalline structures was proposed to co-exist as the nanocrystals grew. However, the $CsPb_2Br_5$ converted back to $CsPbBr_3$ due to the amount of Cs^+ available at high temperatures (ca. 190 °C). As it has been previously reported, $CsPbBr_3$ can evolve to $CsPb_2Br_5$ ($\Delta G < 0$) at temperatures above 123 °C. The authors proposed that $CsPb_2Br_5$ extended to layers on the crystal surface and, at the quenching reaction temperature, it cannot convert back to $CsPbBr_3$ and remain on its surface. Qualitative study of the emission stability in polar medium, such as water and ethanol, were performed in colloidal dispersion and thin films, but the emission quantum yield was not reported.

A $CsPbBr_3$@$CsPb_2Br_5$ core@shell heteronanocrystal has been prepared as powder by the *in situ* outer phase-transition approach, where the presence of water drove the transformation of monoclinic $CsPbBr_3$ NCs to a tetragonal $CsPb_2Br_5$ shell. The small mismatch between both structures favored the epitaxial crystallization interphase. However, these HNCs presented

certain size heterogeneity and a low photoluminescence quantum yield (13 %).[2] Likewise, Zhang et al. reported the preparation of high thermal and water-resistant nano/microspheres of $CsPbBr_3/CsPb_2Br_5$ structures embedded in a thick PbBr(OH) shell by a thorough control of the water content in the reaction media.[26] The PbBr(OH) enhanced the $CsPbBr_3/CsPb_2Br_5$ stability in aqueous media due to its high enthalpy of decomposition in water. Brighter core@shell heteronanocrystals have been prepared as green and red emitters by one-step hot injection core/shell synthesis using a 2.6-fold amount of the lead halide precursor, increasing the reaction time from few seconds to ten minutes and carrying out the process at 210 °C.[4] A contraction on the core size was observed during the formation of the core@shell heteronanocrystal, as evidenced by the lower size observed in the TEM images together with the blue shift in the absorption and emission spectra. These materials produced liquid crystals displays based on perovskite emitters with a higher efficiency than conventional 2-phosphor-converted white light emitting diodes.[4]

Herein, we propose a simple one-pot strategy to prepare highly emissive and stable core@shell heteronanostructures by controlling the temperature of the Cs-oleate precursor solution before the injection, which was the critical step to track the crystalline growth of the ultrathin $CsPb_2Br_5$ coating on the $CsPbBr_3$ core, instead of increasing the amount of toxic lead halide precursor. Indeed, they present long-term stability compared to the pristine $CsPbBr_3$ NCs and can be stored for more than one year (18 months) preserving their chemical and photophysical properties. Furthermore, the $CsPb_2Br_5$ shell acted as a remarkable permeable membrane to monitor the dynamic anion exchange to produce pure $CsPbCl_3@CsPb_2Cl_5$ and $CsPbI_3@CsPb_2I_5$ HNCs with a higher photoluminescence response than the pristine nanocrystals.

EXPERIMENTAL SECTION

Precursors and solvents: All the reagents used in the synthesis of the perovskite NCs were purchased from different commercial suppliers and were used as received. The organic solvents were of spectroscopic grade (from Scharlab, Alfa Aesar and Aldrich).

Reagents: Cesium carbonate (99 %, Sigma Aldrich; Cs_2CO_3), lead bromide (99.999 %, Sigma Aldrich; $PbBr_2$), lead iodide (99.999 %, Sigma Aldrich; PbI_2), lead chloride (99.999 %, Sigma Aldrich; $PbCl_2$) oleylamine (70 %, Sigma Aldrich), oleic acid (90 %, Sigma Aldrich), octadecene (90 %, Alfa Aesar), toluene, hexane and *N*,*N*-dimethylformamide (DMF).

Synthesis of Cs-Oleate: 0.005 mmol of Cs_2CO_3 (1.628g), 20 mL of octadecene, and 5 mL of oleic acid were loaded into a 50 mL 2-neck flask. The precursors were heated in a flask for 1 h at 120 °C and then, the temperature was raised to 150 °C under N_2 atmosphere until the complete solubilization of Cs_2CO_3. Finally, the Cs-oleate solution was stored at 2 °C. In a conventional synthesis, Cs-oleate dispersion must be previously pre-heated before being added to the flask since it precipitates in the ODE solution at room temperature. However, in this methodology, a diluted solution of the Cs precursor in ODE, called "Cs-Ol" was prepared before each perovskite NC synthesis. This solution contained 125 μL of the as-prepared Cs-oleate (0.4 M) described above and 0.5 mL of octadecene and it was kept at room temperature. Adding this extra amount of octadecene allowed us to handle and inject Cs-oleate at room temperature.

Synthesis of $CsPbBr_3$ NCs: For preparing the usual $CsPbBr_3$ NCs, 0.188 mmol of $PbBr_2$ (69 mg) and 25 mL of octadecene were loaded in a 250 mL, 3-neck flask and then dried under vacuum for 1 h at 120 °C. Subsequently, under N_2 atmosphere, 1 mL of oleylamine and 1 mL of oleic acid were injected until the complete solubilization of $PbBr_2$. After 5 minutes, the temperature was raised to 180 °C and the "Cs-Ol" solution, which was previously heated at 65 °C for ca. 20 minutes, was swiftly injected and, right after, the reaction was quenched in an ice-water bath.

The purification of the $CsPbBr_3$ NCs was carried out by two consecutive centrifugation steps. The crude of the reaction was centrifuged at 5000 rpm (10 °C for 5 minutes), and the precipitate obtained was redispersed in 2 mL of hexane:methyl acetate (1:1) mixture to be centrifuged under the same conditions. The $CsPbBr_3$ NCs were isolated in the second precipitate, which was redispersed in 2 mL of hexane for further use and characterization.

Synthesis of core@shell HNCs: For the synthesis of core@shell HNCs, the initial synthetic procedure remained the same. However, "Cs-Ol" solution, kept at room temperature, was injected at 180 ºC, the temperature was rapidly raised to 250 °C (temperature rise ca. 10 minutes) and then, the reaction was promptly quenched in an ice-water bath (about 5 s later). The purification process was performed under the same conditions as for pristine $CsPbBr_3$ NCs.

Stability measurements: The stability of these NCs against different media was evaluated by using diluted NC dispersions, thereby avoiding aggregation effects or delayed degradations because of using highly concentrated samples. Hence, the absorption for all the NC dispersions was set to 0.1 at 365 nm.

- Photostability: The experiments were performed by irradiating the diluted NC sample at 365 nm with a Xenon lamp of 150 W for 9 hours. A soft stirring was used to avoid any interference from NC precipitation.
- Stability in contact with DMF: To 0.5 mL of a diluted NC dispersion in toluene (absorption 0.1 at 365 nm) was added from 0.15 to 0.45 mL of DMF. The emission of both samples was checked after 30 minutes under UV light.
- Stability in contact with water: 0.5 mL of miliQ-water was added to 1.0 mL of the NC diluted sample. The emissive properties of the dispersions were recorded for several days.
- Chemical stability: a fraction of the purified core@shell HNCs was dried under vacuum and the solid was stored for more than a year under ambient conditions. After several months, the perovskite solid was redispersed in toluene to study its optical properties.

Film preparation: films were prepared by using a small amount of the core@shell HNCs, which were stored under dry conditions for 18 months and then dispersed in 200 μL of hexane. Then, all the content was drop-casted in aliquots of 20 μL on top of a 1x1 cm glass substrate. The film was completely dried under ambient atmosphere and fully characterized by optical spectroscopy. The absorption measurements were recorded by using an integration sphere in the reflectance mode, whereas steady-state and time-resolved photoluminescence were registered using a front-face sample holder to properly adjust the film. The quantum yield was measured in an integration sphere with a film holder.

Halide exchange: different halide precursor solutions were prepared for conducting the halide exchange experiments in both the core@shell HNCs and the pristine $CsPbBr_3$ NCs. Firstly, 0.1 mmol of $PbCl_2$ or PbI_2 was mixed with 0.1 mL of oleic acid and 0.1 mL of oleylamine in 5 mL of toluene. Then, the mixture was stirred at 100 °C for 30-60 min until the complete dispersion of the salts.[27-28] Once at room temperature, a few microliters of the precursor solution (in fractions of 20 μL) were added to diluted colloidal dispersions of the NCs to study the halide substitution. The evolution of the process was followed by recording the absorption and photoluminescence spectra of the NCs at different times.

UV-visible spectroscopy: UV-Visible absorption measurements were carried out on a spectrophotometer UV/VIS/NIR Lambda 1050, equipped with software PerkinElmer UV Winlab.

Steady-state and time-resolved photoluminescence (PL): steady-state and time-resolved emission measurements of all the NCs dispersions were recorded in an FLS1000 photoluminescence spectrometer from Edinburgh Instruments. This instrument is equipped with a 450 W ozone-free xenon arc lamp and coupled to a 375 nm picosecond pulsed diode laser (EPL-375, Edinburgh Instruments). The excitation wavelength used for the steady-state

and time-resolved measurements were at 365 nm and 375 nm, respectively. The Fluoracle software was used to register and analyze the data.

Quantum yield: The quantum yield measurements were recorded with a Quantaurus QY Plus C13534-11 from Hamamatsu, equipped with a Xenon lamp for excitation in the UV-visible range.

X-ray Diffraction: The PXRD pattern of all the samples were obtained in a Panalytical Empyrean X-ray platform with a capillarity set-up and copper radiation (Cu Kα = 1.541 78 Å). The capillary tube was made of special glass nº 0140, with a diameter of 0.5 mm.

Transmission electron microscopy. Transmission electron microscopy (TEM) was performed on a HITACHI HT7800 microscope with a filament of LaB6 operated at 100 keV. High resolution images were performed on a FEI TECNAI G2 F20 operated at 200 keV.

Scanning transmission electron microscopy high-angle annular field (STEM-HAADF): images were acquired using a FEI Titan 80-300kV transmission electron microscope (TEM) operated at 300 kV. This microscope is equipped with a condenser lens Cs corrector (CETCOR Cs-condenser CEOS Company) and a high brightness field emission gun (XFEG). The convergent semi-angle was 25 mrad and particular care has been considered for avoiding electron beam damage.

Raman Spectroscopy: Raman measurements were acquired using a Confocal Raman microscope (RMS1000, Edinburgh Instruments). The sample was irradiated using a 638 nm laser focused with a 100x/0.9N.A objective lens. Back scattered light was collected using an 800 mm focal length spectrograph with a 600 gr/mm grating and the Raman spectra were recorded by using an EM-CCD detector.

RESULTS AND DISCUSSION

Herein, a modified hot injection approach was carried out to yield homogeneous and highly emissive $CsPbBr_3$@$CsPb_2Br_5$ core@shell heteronanocrystals. Briefly, oleylamine (OAM) and oleic acid (OA) were loaded in octadecene (ODE) and heated up to 180 ˚C for 5 seconds, followed by the swift addition of a Cs-oleate solution (previously diluted in ODE and maintained at 25 ˚C) and the mixture was heated up to 250 ˚C and maintained at this temperature for 5 sec (Figure 1a). Then, the reaction was cooled down (ice bath) to produce the homogeneous formation of $CsPbBr_3$@$CsPb_2Br_5$ core@shell HNC. In the conventional synthesis of $CsPbBr_3$ NCs by the hot injection strategy, the Cs-oleate solution was heated (at ca. 65 ˚C) to ensure the solubility of the precursor previously to the fast injection into the flask, and the mixture was heated up to 180 ˚C for 5 seconds. Considering our experimental conditions (Cs-oleate injection at 180 °C and heating up to 250°C) the formation of $CsPb_2Br_5$ is thermodynamically favored in agreement with a Gibbs free energy $\Delta G < 0$ observed above 123.5 °C, as has been proposed by Li et al.[14] The partial transformation of $CsPbBr_3$ into $CsPb_2Br_5$ shell could also be favored by the presence of Pb^{2+} and Br^- in the reaction medium at a high reaction temperature, as it was reported by Xu et al.[15] In addition, the availability of Cs^+ in the media (Cs-oleate) would control the reversibility of $CsPb_2Br_5$ to $CsPbBr_3$ to efficiently produce homogeneous HNCs.

The transmission electron microscopy (TEM) images revealed the formation of HNCs with a cuboidal morphology and the total lateral size of 14 ± 2 nm, core of ca. 10 nm and a thin shell of ca. 2.0 nm (Figure 1b and Figures S1a-b). The $CsPbBr_3$ NCs prepared using the conventional strategy yielded cuboids with a length of 9 ± 1 nm (Figure S2a-b), similar to those obtained when the reaction mixture was heated up to 250 °C after the addition of Cs-Ol at 65 °C (9 ± 1 nm, Figure S3 a-b).

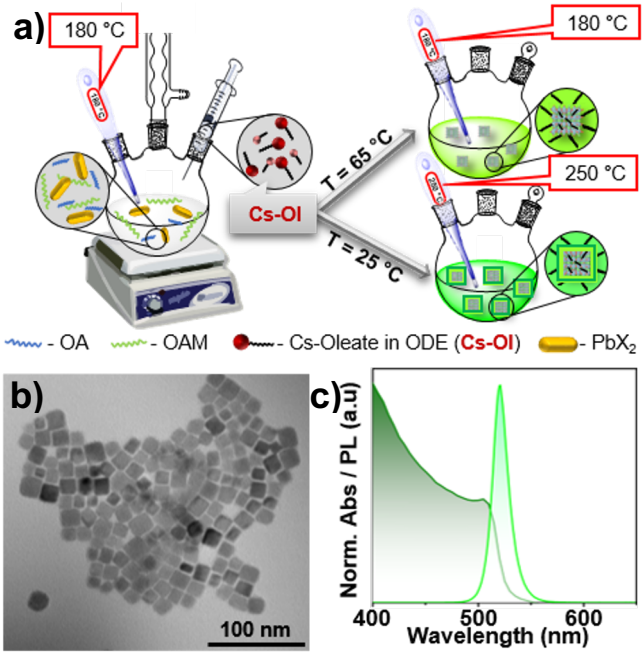

Figure 1. a) Scheme of the synthetic approach for the core NCs and core@shell HNCs using a modified hot injection strategy, b) TEM images of core@shell HNCs, scale bar of 100 nm, and c) normalized absorption and emission spectra of core@shell HNCs.

A close inspection of the high-angle annular dark field-scanning transmission electron microscopy (HAADF-STEM) and the high-resolution transmission electron microscopy (HR-TEM) images (Figure 2a-d and Figure S4 a-b) confirmed the crystallinity of the HNCs and the homogeneous formation of the ultrathin $CsPb_2Br_5$ shell of ~2 nm on the $CsPbBr_3$ NC surface. The inverse fast Fourier transformation (i-FFT) analysis revealed the presence of two main lattice spacing of 0.26 nm and 0.20 nm which correspond to the 310 and 242 crystal planes,

respectively (Figure 2c-d). They can be assigned to the presence of orthorhombic $CsPbBr_3$ and tetragonal $CsPb_2Br_5$, respectively, in the HNCs.[29-30] The additional lattice spacing of 0.42 nm (plane 110) and 0.30 nm (plane 220) was also observed for both components (Figure S4c) as previously reported. [2, 9, 14, 31-34] It is noteworthy that the electron diffraction pattern analysis (Figure S5 and Table S1) only shows the planes corresponding to the orthorhombic $CsPbBr_3$ in the HNCs, while the planes of tetragonal $CsPb_2Br_5$ were not detected, this is consistent with the presence of a very thin shell layer.

XRD analyses were performed to validate the presence of both structures in the HNCs (Figure 2e). The reflections observed at 11.61, 23.98, 29.35 and 33.33 were attributed to the (002), (210), (213), and (312) planes of tetragonal $CsPb_2Br_5$, respectively.[35] Furthermore, the characteristic peaks of orthorhombic $CsPbBr_3$ NCs at 15.19, 21.45, 30.67 and 37.85, assigned to the (101), (121), (202) and (321) planes were also observed (COD ID 1533062), thus confirming the formation of $CsPbBr_3$@$CsPb_2Br_5$ core@shell HNCs.[36] Figure 2f-g illustrates the crystalline structure of both materials present in the HNCs; the orthorhombic $CsPbBr_3$ NCs, which are composed by interconnected $[PbBr_6]^{4-}$ octahedra, and the tetragonal $CsPb_2Br_5$, made up of quasi-2D periodic $[Pb_2Br_5]^-$ layers separated by Cs^+ layers.[2]

High-resolution X-ray photoelectron spectroscopy (XPS) was used to analyze the interaction between the core and the shell components in the HNCs. The binding energy of C1s (284.6 eV) was set to adjust the XPS spectra of the relevant elements, specifically Cs, Pb and Br (Figure 2 h-j). The peaks of the three elements shifted to higher binding energy concomitantly with a broadening of the signals (Table S2). The Pb 4f core level spectrum of pristine $CsPbBr_3$ showed two peaks located at 137.8 eV and 142.7 eV, assigned to the Pb $4f_{7/2}$ and Pb $4f_{5/2}$ levels, respectively. [3, 37] These peaks shifted to higher energy and were observed at 138.7 eV and 143.6 eV in the HNC (ΔeV = 0.9 eV), thereby suggesting a lower electron density in the $CsPbBr_3$

NCs after the addition of the shell, as it has recently reported for a $CsPbBr_3/CsPb_2Br_5$ composite.[3] A similar behavior, but at lower magnitude was obtained for Br and Cs species. The binding energy peaks registered at 67.8 eV and 68.8 eV in the pristine $CsPbBr_3$, assigned to Br $3d_{5/2}$ and Br $3d_{3/2}$ levels, respectively,[33] slightly shifted to a higher energy ($\Delta eV = 0.7$ eV). In the case of the Cs 3d, the binding energy peaks were observed at 724 eV and 737.9 eV in the $CsPbBr_3$ NCs, which can be attributed to Cs $3d_{3/2}$ and Cs $3d_{5/2}$ levels, respectively, positively shifted ($\Delta eV = 0.3$ eV). A similar shift (ca. 0.15-0.2 eV) has also been reported for i) $CsPbBr_3@CsPb_2Br_5$ powder composites, generated by partial conversion of the $CsPbBr_3$ cubic phase into the $CsPb_2Br_5$ tetragonal phase in a process mediated by water[38] and ii) the 0D $CsPbBr_3$/2D $CsPb_2Br_5$ assembly, where the shifting in the binding energy was attributed to the strong co-sharing of the active atoms (mainly Pb) between 0D $CsPbBr_3$ and 2D $CsPb_2Br_5$ nanosheets.[3, 38]

Raman spectroscopy was also recorded to gain more information about the heteronanocrysal structure. The Raman spectra recorded at 638 nm excitation (Figure S6) revealed the presence of the peak at 313 cm^{-1}, which is typical of $CsPbBr_3$ NCs.[2, 39] This peak is absent in the HNC spectrum, thereby confirming the complete covering of the pristine NCs with the shell of $CsPb_2Br_5$. This has been described for similar $CsPbBr_3@CsPb_2Br_5$ HNCs, but with less homogeneity in the encapsulation of the core and the HNC size.[2] The Raman spectra of the HNCs evidenced two main sharp peaks at 88 cm^{-1} and 143 cm^{-1}, attributed to the presence of $CsPb_2Br_5$.[2] The slight shift of the main peaks towards a higher energy is consistent with a strong interaction between the core and the shell in the HNC, corroborating the XPS findings (see Figure 2).

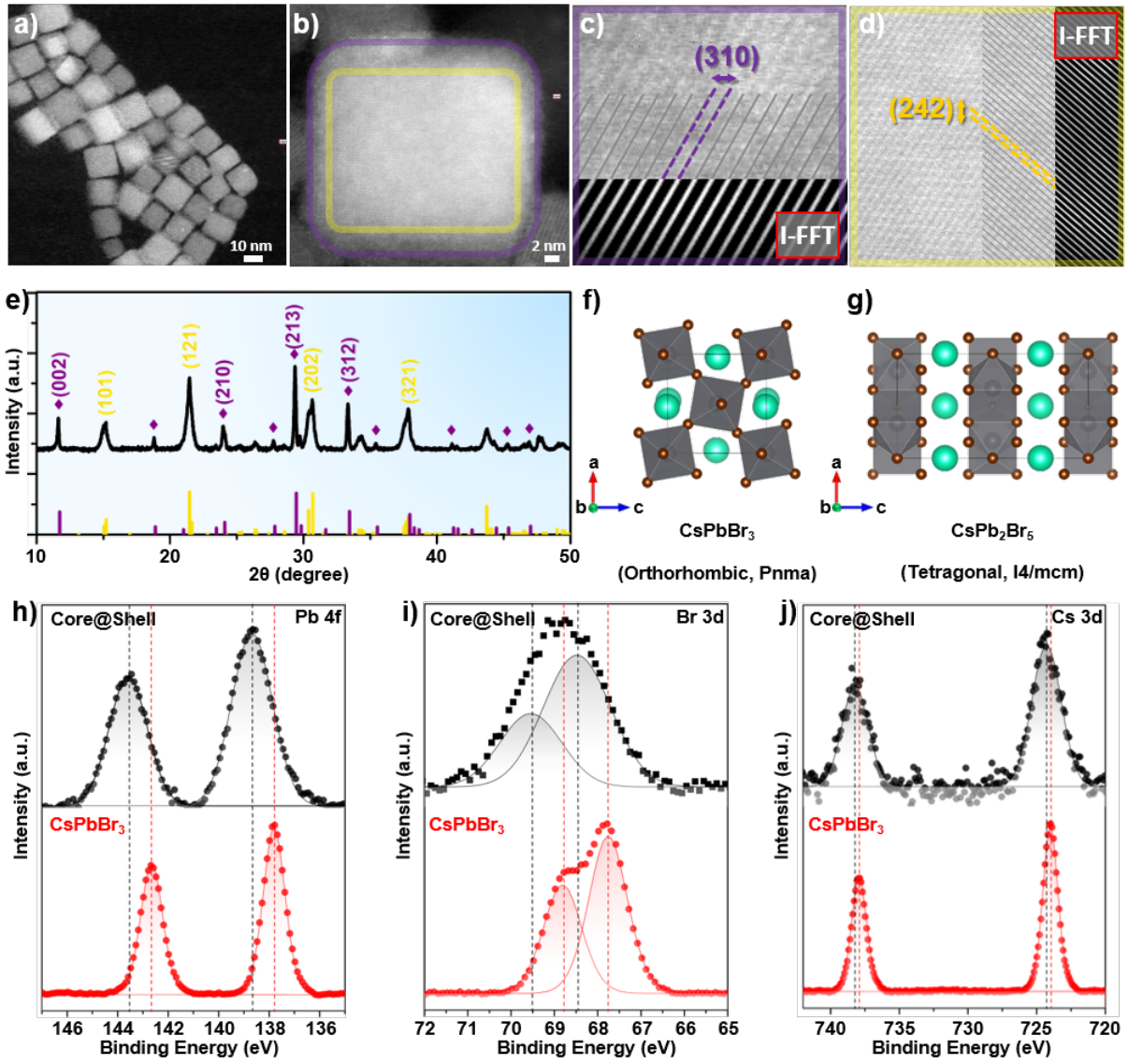

Figure 2. a) HAADF-STEM image of the $CsPbBr_3$@$CsPb_2Br_5$ HNCs sample, and b) enlarged image of a heteronanocrystal highlighting the core@shell area ($CsPb_2Br_5$-shell and $CsPbBr_3$-core in purple and yellow, respectively). Selected areas of the image including the inversed fast Fourier transformation (I-FFT region) of c) the (310) and d) the (242) planes ascribed to the $CsPb_2Br_5$ shell and $CsPbBr_3$ core, respectively. e) XRD patterns of core@shell HNCs with the corresponding reflection peaks of orthorhombic $CsPbBr_3$ (COD ID 1533062 – yellow line) and tetragonal $CsPb_2Br_5$ (calculated XRD spectra extracted from ref. 35 – purple line). f) Crystal structure of the orthorhombic $CsPbBr_3$ and tetragonal $CsPb_2Br_5$. XPS spectra of h) Pb 4f, i) Br 3d and j) Cs 3d for the core@shell HNCs (black line) and $CsPbBr_3$ NCs (red line).

The optical features of the core@shell HNCs disclose a maximum at 510 nm and 519 nm in the absorption and emission spectra, respectively (Figure 1c, Table S3, entry 1). These values are slightly red shifted compared to those of the pristine $CsPbBr_3$ NCs (obtained by the conventional protocol: heated up to 180 °C or 250 °C) at 503 nm and 511 nm (Figure S2c, Figure S3c and Table S3). Interestingly, a full with at half maximum (FWHM) of 17 nm was calculated for the core@shell HNCs, compared to 19-20 nm observed for the pristine NCs and previously reported for core@shell systems.[4] This is consistent with a narrower size distribution of the obtained HNCs and their higher color purity as compared to the pristine NCs.

The photoluminescence quantum yield (Φ_{PL}) of the core $CsPbBr_3$ NCs increased by 30 % (from 51 % up to 65 %) in the core@shell HNCs, thus suggesting a good passivation of the core surface defects. This fact was consistent with the observed decrease in the non-radiative decay rate (k_{nr}), from 8.2 10^7 s^{-1} to 4.8 10^7 s^{-1} (Table S4), while the radiative decay rate (k_r) value maintained. The PL lifetimes fitted to a triexponential function and the average lifetime (τ_{av}) increased from 5.9 ns to 7.3 ns after the formation of the shell (Figure S7). This result was opposite to the lifetime decrease observed for the $CsPbBr_3$@$CsPb_2Br_5$ core@shell heteronanocrystal powder with wider shells (10-20 nm); this has been attributed to the stronger spatial carrier confinement caused by the potential barrier of the $CsPb_2Br_5$ shell.[2]

Lengthening of the PL lifetime could be attributed to the reduction of defects after the inorganic coating of the core, thereby mitigating the non-radiative recombination; as was previously reported for core@shell like structure.[15] The PL excitation spectra of the core@shell HNCs showed a high energy peak at 3.61 eV (Figure S8) assigned to the excitonic peak of $CsPb_2Br_5$, which present a bigger band gap compared to that of the pristine NCs. Additional peaks at 3.9 eV were also attributed to the presence of the ultrathin $CsPb_2Br_5$ shell.[2]

The combination of high photoluminescence quantum yield and narrow FWHM makes these HNCs good materials for PLED applications. Although they manifest excellent optical properties, the stability under light and polar solvents remains a challenge. Therefore, the colloidal stability of the core and core-shell NCs and their emissive properties were studied under continuous UV light (365 nm) irradiation for 9 h (Figure 3 a-b). The core NCs showed a decrease in the Φ_{PL} of 10 %, while the core@shell HNCs displayed an enhancement of the emission of 7 %. The stability of the core NCs and core@shell HNCs dispersed in toluene and in close contact with water was studied for 240 h (Figure 3c). The emission decreased to ca. 5% (Φ_{PL} 3.5) in the core@shell HNCs, while the core NC emission was completely quenched after only 24 h. Figure 3d shows the picture of core@shell HNCs dispersed in toluene after being kept in contact with dimethylformamide for 30 minutes, compared to the core NCs under otherwise the same conditions. Clearly the HNC partially retained its emission, while the core NC was not emissive. It is noteworthy that the core@shell HNCs preserved the shape after contact with DMF, while the core NCs exhibited clear degradation (see TEM images in Figure S9). Regarding the long-term chemical stability, the core@shell HNCs were stored for 18 months in solid state under ambient conditions and then, a small amount of the powder was redispersed in toluene maintaining the same optical features (Table S3, entry 4) and morphology (Figure S10) than the as-prepared. In the case of core NCs, the maxima of the absorption and emission experimented a significant red shift (Table S3, entry 5)

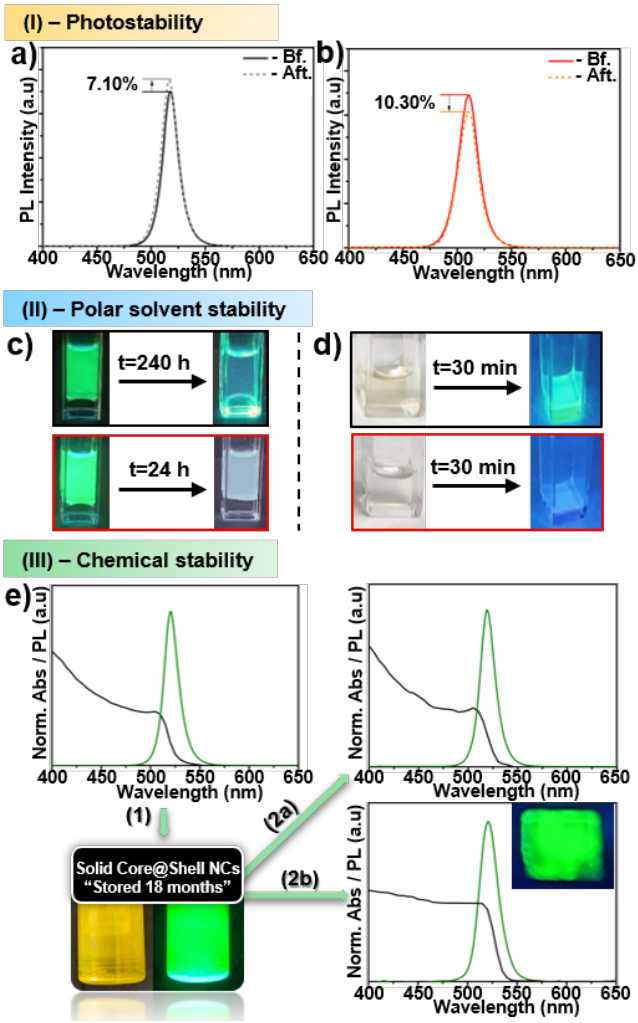

Figure 3. (I) – Photostability analysis: Evolution of the emission spectra of the a) core@shell HNCs and b) $CsPbBr_3$ NCs after 9 hours of continuous irradiation at 365 nm (150 W). (II) – Stability analysis in a polar solvent: c) emission under UV light of the core@shell HNC (black frame) and $CsPbBr_3$ NC (red frame) toluene dispersions in contact with water for 240 and 24 hours, respectively. d) Images of the core@shell HNC (black frame) and $CsPbBr_3$ NC (red frame) toluene dispersions in contact with DMF, taken under laboratory and UV light. (III) - Chemical stability: e) Absorption and emission spectra of core@shell HNCs before (1) storing them dried under ambient conditions for 18 months, (2a) absorption, emission spectra after their redispersion in toluene and (2b) film prepared in a glass substrate (inset image of the film emission under UV-light).

The redispersed core@shell HNCs were also used to prepare a thin film by drop casting. The film presented similar absorption and emission properties to that of the initial HNCs (Table S3, entry 6 and Figure S11).

We further studied the permeability of the shell to ions such as Cl^- or I^- by using the halide exchange strategy[27-28] and the partial or total incorporation of the halides was evaluated (Figure 4a). The emission spectrum of the $CsPbBr_3/CsPb_2Br_5$ HNC toluene dispersion was recorded after the addition of increasing concentrations of $PbCl_2$ or PbI_2 ($4 \cdot 10^{-7}$-$1.2 \cdot 10^{-6}$ mol). An emission band at 415 nm appeared after the addition of $PbCl_2$ and the intensity increased with Cl^- concentration with the concomitant decrease of the green emission (Figure 4b). Interestingly, the emission Φ_{PL} enhanced up to 51% after 18 h of stabilization. It is noteworthy that the halide exchange of Br^- by Cl^- was extraordinarily fast (shift from 519 nm to 415 nm) in comparison with the progressive shift observed after the addition of PbI_2 to provide red emissive HNCs with a maximum at 677 nm and an emission quantum yield of 84% (Figure 4c). The different anion exchange dynamics could be ascribed to the relative atomic radius of the halides: Cl^- (100 pm) and I (140 pm) to replace pristine Br^- (115 pm).[40] Remarkably, the halide exchange to the pristine $CsPbBr_3$ NCs produced a similar emission maximum, but the Φ_{PL} was 29% and 66% after the incorporation of Cl^- and I^-, respectively (Figure S12). Moreover, the addition of $4 \cdot 10^{-7}$ mol of the $PbCl_2$ was enough to observe a complete exchange of Br^- by Cl^-. The absorption spectra before and after the halide exchange are illustrated in Figure S13. In both cases the exciton peak of the core shifted from 509 nm to 409 nm and 667 nm after the exchange with Cl^- and I^-, respectively.

The addition of increasing concentrations of PbI_2 to the core@shell HNCs resulted in the growing of a band at ca. 450 nm (Figure S13 b) that can be ascribed to the excitonic peak of $CsPb_2I_5$, already reported in $CsPb_2I_5$ materials,[41-43] thereby confirming the total exchange of the halogen anion of the HNCs from Br^- to I^- in both the core and the shell. In fact, the 450 nm

band was absent after the halide exchange in the pristine NCs and the absorption spectra of pristine NCs after the halide exchange showed a maximum at 410 nm and 670 nm for the Cl^- and I^-, respectively (Figure S14).

Figure 4d illustrate the XRD spectra after the halide exchange. There was a clear shift from 21.45 degrees (121) of the orthorhombic $CsPbBr_3$ core to 22.16 degrees and 20.27 degrees, thereby confirming the incorporation of Cl^- and I^-, respectively. However, the peak at 29.35 ascribed to the (213) plane of the $CsPb_2Br_5$ shell was slightly shifted to 29.36 and 29.33 after the halide exchange, that seems to be less sensitive to the halide.[41, 44]

The HR-TEM images of the core@shell HNCs were recorded after the addition of $1.2 \cdot 10^{-6}$ mol of the lead halide precursor solution and 18 hours of stabilization (Figure S15-S16). It should be noted that the morphology of the core@shell HNCs preserved after the halide exchange, thus confirming for the first time that this methodology is a good alternative to prepare pure $CsPbCl_3$@$CsPb_2Cl_5$ and $CsPbI_3$@$CsPb_2I_5$ heteronanocrystals. All these data suggest that the halide exchange in the core@shell HNCs was complete and prove the excellent permeability of the shell to halides, acting as a membrane, to replace the bromide in the core and in the shell in a moderate time by using a high concentration of $PbCl_2$ and PbI_2 salts.

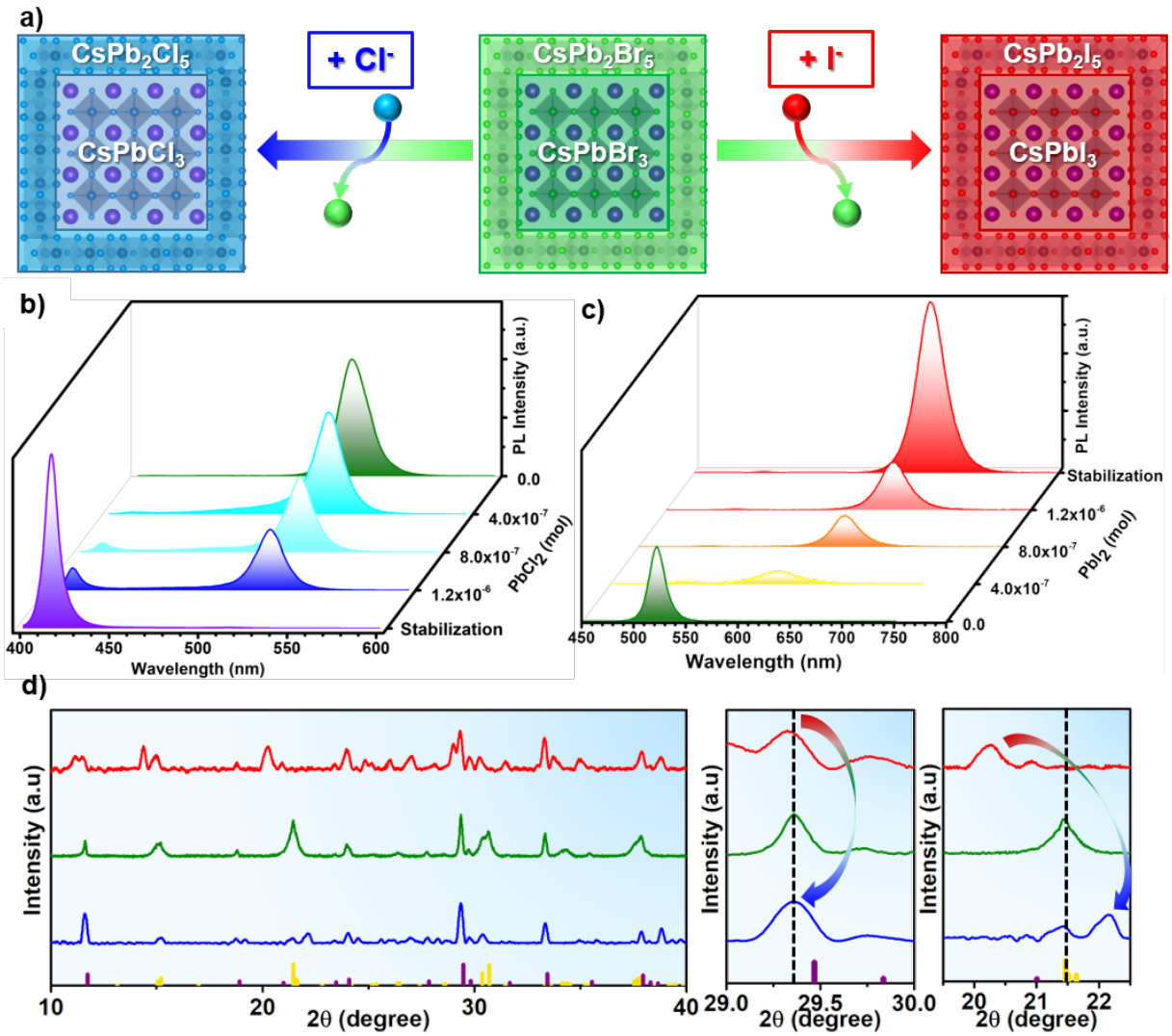

Figure 4. a) Schematic illustration of the halide exchange process for the core@shell HNCs. Emission spectra evolution after the addition of different amounts of b) $PbCl_2$ and c) PbI_2, and a stabilization step of 18 hours. d) XRD spectra of iodide (red line), bromide (green line) and chloride (blue line) core@shell HNCs after the halide exchange reaction together with zooms in specific regions to monitor the shift of the $CsPb_2X_5$ and $CsPbX_3$ perovskites. Comparison of the XRD reflection patterns to those of the bulk material of orthorhombic $CsPbBr_3$ (COD ID 1533062 – yellow line) and tetragonal $CsPb_2Br_5$ (calculated XRD spectra extracted from ref. 35 – purple line).

CONCLUSIONS

In summary, we have prepared emissive and long-term stable core-shell HNCs using a modified one-pot hot injection methodology. The controlled growth of a $CsPb_2Br_5$ shell on the $CsPbBr_3$ NCs was able to reduce the number of defects, such as dangling bonds or halide vacancies, that potentially can trap the photogenerated charges, thereby increasing the photoluminescence quantum yield compared to that of the pristine core NCs. The great permeability of the shell resulted in the formation of pure and emissive $CsPbCl_3$@$CsPb_2Cl_5$ and $CsPbI_3$@$CsPb_2I_5$ heteronanocrystals that, after the halide exchange, do not only preserve the morphology of the pristine NCs, but also improve the emissive response compared to the related core. This is an example of engineering the surface of the NCs with an ultrathin shell to open the way for developing novel perovskite/perovskite heterostructures with low lattice mismatch and higher stability towards external factors, such as light and polar media.

ASSOCIATED CONTENT

Supporting Information.

Additional TEM and HAADF-STEM images, electron diffraction pattern, raman spectra and TRPL spectra of the core@shell HNCs and core NCs. Optical properties, elemental mapping of elements and TEM / HR-TEM images after the halide exchange reactions.

AUTHOR INFORMATION

Corresponding Author

Raquel E. Galian - Institute of Molecular Science, University of Valencia c/ Cat. José Beltrán 2, Paterna, 46980, Valencia, Spain.

ORCID: 0000-0001-8703-4403

Email: Raquel.galian@uv.es

Julia Pérez-Prieto - Institute of Molecular Science, University of Valencia c/ Cat. José Beltrán 2, Paterna, 46980, Valencia, Spain.

ORCID: 0000-0002-5833-341X

Email: julia.perez@uv.es

Author Contributions

The manuscript was written through the contributions of all authors. All authors have given approval to the final version of the manuscript.

Funding Sources

We thank the Spanish Ministry of Science and Innovation (MICINN), projects PID2020115710GB-I00, Agencia Estatal de Investigación-AEI and MICIU Unit of Excellence "Maria de Maeztu" CEX2019-000919-M, as well as the Generalitat Valenciana projects PROMETEO/2019/80, IDIFEDER/2018/064 and IDIFEDER/2021/064, all of which partially co-financed this work with FEDER funds. I.R-P. and A.C. acknowledge the support from the Spanish Ministry of Science, Innovation, and Universities (FPU17/05564, CIGRIS/2021/094). R.A. acknowledges financial support from the Spanish Ministry of Science and Innovation MCIN and the Spanish Research Agency AEI (PID2019-104739GB-100/AEI/10.13039/501100011033), Gobierno de Aragon (DGA, E13-20R), and from the European Union H2020 programs "ESTEEM3" (grant agreement No 823717).

ACKNOWLEDGMENT

The STEM measurements were performed in the Laboratorio de Microscopicas Avanzadas (LMA) at the Universidad de Zaragoza (Spain).

REFERENCES

1. Dey, A.; Ye, J.; De, A.; Debroye, E.; Ha, S. K.; Bladt, E.; Kshirsagar, A. S.; Wang, Z.; Yin, J.; Wang, Y.; Quan, L. N.; Yan, F.; Gao, M.; Li, X.; Shamsi, J.; Debnath, T.; Cao, M.; Scheel, M. A.; Kumar, S.; Steele, J. A.; Gerhard, M.; Chouhan, L.; Xu, K.; Wu, X.-g.; Li, Y.; Zhang, Y.; Dutta, A.; Han, C.; Vincon, I.; Rogach, A. L.; Nag, A.; Samanta, A.; Korgel, B. A.; Shih, C.-J.; Gamelin, D. R.; Son, D. H.; Zeng, H.; Zhong, H.; Sun, H.; Demir, H. V.; Scheblykin, I. G.; Mora-Seró, I.; Stolarczyk, J. K.; Zhang, J. Z.; Feldmann, J.; Hofkens, J.; Luther, J. M.; Pérez-Prieto, J.; Li, L.; Manna, L.; Bodnarchuk, M. I.; Kovalenko, M. V.; Roeffaers, M. B. J.; Pradhan, N.; Mohammed, O. F.; Bakr, O. M.; Yang, P.; Müller-Buschbaum, P.; Kamat, P. V.; Bao, Q.; Zhang, Q.; Krahne, R.; Galian, R. E.; Stranks, S. D.; Bals, S.; Biju, V.; Tisdale, W. A.; Yan, Y.; Hoye, R. L. Z.; Polavarapu, L., State of the Art and Prospects for Halide Perovskite Nanocrystals. *ACS Nano* **2021,** *15* (7), 10775-10981.
2. Liang, T.; Liu, W.; Liu, X.; Li, Y.; Wu, W.; Fan, J., In Situ Phase-Transition Crystallization of All-Inorganic Water-Resistant Exciton-Radiative Heteroepitaxial $CsPbBr_3$–$CsPb_2Br_5$ Core–Shell Perovskite Nanocrystals. *Chem. Mater.* **2021,** *33* (13), 4948-4959.
3. Ding, L.; Borjigin, B.; Li, Y.; Yang, X.; Wang, X.; Li, H., Assembling an Affinal 0D $CsPbBr_3$/2D $CsPb_2Br_5$ Architecture by Synchronously In Situ Growing $CsPbBr_3$ QDs and $CsPb_2Br_5$ Nanosheets: Enhanced Activity and Reusability for Photocatalytic CO_2 Reduction. *ACS Applied Materials & Interfaces* **2021,** *13* (43), 51161-51173.
4. Yoon, H. C.; Lee, H.; Kang, H.; Oh, J. H.; Do, Y. R., Highly efficient wide-color-gamut QD-emissive LCDs using red and green perovskite core/shell QDs. *Journal of Materials Chemistry C* **2018,** *6* (47), 13023-13033.
5. Bera, S.; Pradhan, N., Perovskite Nanocrystal Heterostructures: Synthesis, Optical Properties, and Applications. *ACS Energy Letters* **2020,** *5* (9), 2858-2872.
6. Smith, A. M.; Nie, S., Semiconductor Nanocrystals: Structure, Properties, and Band Gap Engineering. *Acc. Chem. Res.* **2010,** *43* (2), 190-200.
7. Ahmed, G. H.; Yin, J.; Bakr, O. M.; Mohammed, O. F., Successes and Challenges of Core/Shell Lead Halide Perovskite Nanocrystals. *ACS Energy Letters* **2021,** *6* (4), 1340-1357.
8. Dirin, D. N.; Benin, B. M.; Yakunin, S.; Krumeich, F.; Raino, G.; Frison, R.; Kovalenko, M. V., Microcarrier-Assisted Inorganic Shelling of Lead Halide Perovskite Nanocrystals. *ACS Nano* **2019,** *13* (10), 11642-11652.
9. Jiang, G.; Guhrenz, C.; Kirch, A.; Sonntag, L.; Bauer, C.; Fan, X.; Wang, J.; Reineke, S.; Gaponik, N.; Eychmüller, A., Highly Luminescent and Water-Resistant $CsPbBr_3$–$CsPb_2Br_5$ Perovskite Nanocrystals Coordinated with Partially Hydrolyzed Poly(methyl methacrylate) and Polyethylenimine. *ACS Nano* **2019,** *13* (9), 10386-10396.
10. Ravi, V. K.; Saikia, S.; Yadav, S.; Nawale, V. V.; Nag, A., $CsPbBr_3$/ZnS Core/Shell Type Nanocrystals for Enhancing Luminescence Lifetime and Water Stability. *ACS Energy Letters* **2020,** *5* (6), 1794-1796.
11. Shamsi, J.; Dang, Z.; Ijaz, P.; Abdelhady, A. L.; Bertoni, G.; Moreels, I.; Manna, L., Colloidal CsX (X = Cl, Br, I) Nanocrystals and Their Transformation to $CsPbX_3$ Nanocrystals by Cation Exchange. *Chem. Mater.* **2018,** *30* (1), 79-83.
12. Kaur, G.; Justice Babu, K.; Ghorai, N.; Goswami, T.; Maiti, S.; Ghosh, H. N., Polaron-Mediated Slow Carrier Cooling in a Type-1 3D/0D $CsPbBr_3$@Cs_4PbBr_6 Core–Shell Perovskite System. *The Journal of Physical Chemistry Letters* **2019,** *10* (18), 5302-5311.
13. Wang, B.; Zhang, C.; Huang, S.; Li, Z.; Kong, L.; Jin, L.; Wang, J.; Wu, K.; Li, L., Postsynthesis Phase Transformation for $CsPbBr_3$/Rb_4PbBr_6 Core/Shell Nanocrystals with Exceptional Photostability. *ACS Applied Materials & Interfaces* **2018,** *10* (27), 23303-23310.

14. Li, G.; Wang, H.; Zhu, Z.; Chang, Y.; Zhang, T.; Song, Z.; Jiang, Y., Shape and phase evolution from $CsPbBr_3$ perovskite nanocubes to tetragonal $CsPb_2Br_5$ nanosheets with an indirect bandgap. *Chem. Commun.* **2016,** *52* (75), 11296-11299.
15. Qiao, B.; Song, P.; Cao, J.; Zhao, S.; Shen, Z.; Di, G.; Liang, Z.; Xu, Z.; Song, D.; Xu, X., Water-resistant, monodispersed and stably luminescent $CsPbBr_3/CsPb_2Br_5$ core–shell-like structure lead halide perovskite nanocrystals. *Nanotechnology* **2017,** *28* (44), 445602.
16. Zhang, X.; Xu, B.; Zhang, J.; Gao, Y.; Zheng, Y.; Wang, K.; Sun, X. W., All-Inorganic Perovskite Nanocrystals for High-Efficiency Light Emitting Diodes: Dual-Phase $CsPbBr_3$-$CsPb_2Br_5$ Composites. *Adv. Funct. Mater.* **2016,** *26* (25), 4595-4600.
17. Schmidt, L. C.; Pertegás, A.; González-Carrero, S.; Malinkiewicz, O.; Agouram, S.; Mínguez Espallargas, G.; Bolink, H. J.; Galian, R. E.; Pérez-Prieto, J., Nontemplate Synthesis of $CH_3NH_3PbBr_3$ Perovskite Nanoparticles. *J. Am. Chem. Soc.* **2014,** *136* (3), 850-853.
18. Gonzalez-Carrero, S.; Galian, R. E.; Pérez-Prieto, J., Maximizing the emissive properties of $CH_3NH_3PbBr_3$ perovskite nanoparticles. *Journal of Materials Chemistry A* **2015,** *3* (17), 9187-9193.
19. Protesescu, L.; Yakunin, S.; Bodnarchuk, M. I.; Krieg, F.; Caputo, R.; Hendon, C. H.; Yang, R. X.; Walsh, A.; Kovalenko, M. V., Nanocrystals of Cesium Lead Halide Perovskites ($CsPbX_3$, X = Cl, Br, and I): Novel Optoelectronic Materials Showing Bright Emission with Wide Color Gamut. *Nano Lett.* **2015,** *15* (6), 3692-3696.
20. Rosa-Pardo, I.; Cortés-Villena, A.; Galian, R. E.; Pérez-Prieto, J., Chapter 4 - Synthesis techniques of metal halide perovskites. In *Low-Dimensional Halide Perovskites*, Zhan, Y.; Khalid, M.; Vivo, P.; Arshid, N., Eds. Elsevier: 2023; pp 91-151.
21. Wen, J.-R.; Roman, B. J.; Rodriguez Ortiz, F. A.; Mireles Villegas, N.; Porcellino, N.; Sheldon, M., Chemical Availability of Bromide Dictates $CsPbBr_3$ Nanocrystal Growth. *Chem. Mater.* **2019,** *31* (20), 8551-8557.
22. Vighnesh, K.; Wang, S.; Liu, H.; Rogach, A. L., Hot-Injection Synthesis Protocol for Green-Emitting Cesium Lead Bromide Perovskite Nanocrystals. *ACS Nano* **2022,** *16* (12), 19618-19625.
23. Lu, C.; Wright, M. W.; Ma, X.; Li, H.; Itanze, D. S.; Carter, J. A.; Hewitt, C. A.; Donati, G. L.; Carroll, D. L.; Lundin, P. M.; Geyer, S. M., Cesium Oleate Precursor Preparation for Lead Halide Perovskite Nanocrystal Synthesis: The Influence of Excess Oleic Acid on Achieving Solubility, Conversion, and Reproducibility. *Chem. Mater.* **2019,** *31* (1), 62-67.
24. Zhang, X.; Lin, H.; Huang, H.; Reckmeier, C.; Zhang, Y.; Choy, W. C. H.; Rogach, A. L., Enhancing the Brightness of Cesium Lead Halide Perovskite Nanocrystal Based Green Light-Emitting Devices through the Interface Engineering with Perfluorinated Ionomer. *Nano Lett.* **2016,** *16* (2), 1415-1420.
25. Rodová, M.; Brožek, J.; Knížek, K.; Nitsch, K., Phase transitions in ternary caesium lead bromide. *J. Therm. Anal. Calorim.* **2003,** *71* (2), 667-673.
26. Du, K.; He, L.; Song, S.; Feng, J.; Li, Y.; Zhang, M.; Li, H.; Li, C.; Zhang, H., In Situ Embedding Synthesis of Highly Stable $CsPbBr_3/CsPb_2Br_5$@PbBr(OH) Nano/Microspheres through Water Assisted Strategy. **2021,** *31* (36), 2103275.
27. Tong, Y.; Bohn, B. J.; Bladt, E.; Wang, K.; Müller-Buschbaum, P.; Bals, S.; Urban, A. S.; Polavarapu, L.; Feldmann, J., From Precursor Powders to $CsPbX_3$ Perovskite Nanowires: One-Pot Synthesis, Growth Mechanism, and Oriented Self-Assembly. *Angew. Chem. Int. Ed.* **2017,** *56* (44), 13887-13892.
28. Rosa-Pardo, I.; Cevallos-Toledo, R. B.; Polavarapu, L.; Arenal, R.; Galian, R. E.; Pérez-Prieto, J., Revisiting the nontemplate approach for the synthesis of highly green emissive hybrid perovskite nanocrystals: platelets or spheres? *Nanoscale* **2022,** *14* (4), 1160-1164.

29. Tenailleau, C.; Aharon, S.; Cohen, B.-E.; Etgar, L., Cell refinement of $CsPbBr_3$ perovskite nanoparticles and thin films. *Nanoscale Advances* **2019,** *1* (1), 147-153.
30. Sun, X.; Gao, Z.; Zhang, W.; Liu, Y.; Xu, B.; Wang, Z.; Wang, X.; Meng, X., Lasing from solution-processed $CsPbBr_3$ octahedral resonators. *J. Lumin.* **2021,** *229*, 117713.
31. Collantes, C.; González Pedro, V.; Bañuls, M.-J.; Maquieira, Á., Monodispersed $CsPb_2Br_5$@SiO_2 Core–Shell Nanoparticles as Luminescent Labels for Biosensing. *ACS Applied Nano Materials* **2021,** *4* (2), 2011-2018.
32. Han, C.; Li, C.; Zang, Z.; Wang, M.; Sun, K.; Tang, X.; Du, J., Tunable luminescent $CsPb_2Br_5$ nanoplatelets: applications in light-emitting diodes and photodetectors. *Photon. Res.* **2017,** *5* (5), 473-480.
33. Wang, R.; Li, Z.; Li, S.; Wang, P.; Xiu, J.; Wei, G.; Liu, H.; Jiang, N.; Liu, Y.; Zhong, M., All-Inorganic Perovskite $CsPb_2Br_5$ Nanosheets for Photodetector Application Based on Rapid Growth in Aqueous Phase. *ACS Applied Materials & Interfaces* **2020,** *12* (37), 41919-41931.
34. Balakrishnan, S. K.; Kamat, P. V., Ligand Assisted Transformation of Cubic $CsPbBr_3$ Nanocrystals into Two-Dimensional $CsPb_2Br_5$ Nanosheets. *Chem. Mater.* **2018,** *30* (1), 74-78.
35. Dursun, I.; De Bastiani, M.; Turedi, B.; Alamer, B.; Shkurenko, A.; Yin, J.; El-Zohry, A. M.; Gereige, I.; AlSaggaf, A.; Mohammed, O. F.; Eddaoudi, M.; Bakr, O. M., $CsPb_2Br_5$ Single Crystals: Synthesis and Characterization. *ChemSusChem* **2017,** *10* (19), 3746-3749.
36. Hudait, B.; Dutta, S. K.; Patra, A.; Nasipuri, D.; Pradhan, N., Facets Directed Connecting Perovskite Nanocrystals. *J. Am. Chem. Soc.* **2020,** *142* (15), 7207-7217.
37. Thapa, S.; Bhardwaj, K.; Basel, S.; Pradhan, S.; Eling, C. J.; Adawi, A. M.; Bouillard, J.-S. G.; Stasiuk, G. J.; Reiss, P.; Pariyar, A.; Tamang, S., Long-term ambient air-stable cubic $CsPbBr_3$ perovskite quantum dots using molecular bromine. *Nanoscale Advances* **2019,** *1* (9), 3388-3391.
38. Gao, P.; Cui, Z.; Liu, X.; Wu, Y.; Zhang, Q.; Wang, Z.; Zheng, Z.; Cheng, H.; Liu, Y.; Li, Q.; Huang, B.; Wang, P., In Situ Preparation of $CsPbBr_3$@$CsPb_2Br_5$ Composite Assisted with Water as a Highly Efficient and Stable Catalyst for Photothermal CO2 Hydrogenation. *Chemistry – A European Journal* **2022,** *28* (50), e202201095.
39. Ibaceta-Jaña, J.; Muydinov, R.; Rosado, P.; Mirhosseini, H.; Chugh, M.; Nazarenko, O.; Dirin, D. N.; Heinrich, D.; Wagner, M. R.; Kühne, T. D.; Szyszka, B.; Kovalenko, M. V.; Hoffmann, A., Vibrational dynamics in lead halide hybrid perovskites investigated by Raman spectroscopy. *PCCP* **2020,** *22* (10), 5604-5614.
40. Slater, J. C., Atomic Radii in Crystals. *The Journal of Chemical Physics* **2004,** *41* (10), 3199-3204.
41. Qin, C.; Matsushima, T.; Sandanayaka, A. S. D.; Tsuchiya, Y.; Adachi, C., Centrifugal-Coated Quasi-Two-Dimensional Perovskite $CsPb_2Br_5$ Films for Efficient and Stable Light-Emitting Diodes. *The Journal of Physical Chemistry Letters* **2017,** *8* (21), 5415-5421.
42. Zhang, B.; Zhang, H.; Lin, J.; Cheng, X., A time-dependent density functional study on optical response in all-inorganic lead-halide perovskite nanostructures. *Int. J. Quantum Chem* **2020,** *120* (13), e26232.
43. Li, M.; Peng, S.; Fang, S.; Gong, Y.; Yang, D.; Bu, K.; Liu, B.; Luo, H.; Guo, S.; Li, J.; Wang, H.; Liu, Y.; Jiang, S.; Lin, C.; Lü, X., Synthesis of Two-Dimensional $CsPb_2X_5$ (X = Br and I) with a Stable Structure and Tunable Bandgap by $CsPbX_3$ Phase Separation. *The Journal of Physical Chemistry Letters* **2022,** *13* (11), 2555-2562.
44. Wang, K.-H.; Wu, L.; Li, L.; Yao, H.-B.; Qian, H.-S.; Yu, S.-H., Large-Scale Synthesis of Highly Luminescent Perovskite-Related $CsPb_2Br_5$ Nanoplatelets and Their Fast Anion Exchange. *Angew. Chem. Int. Ed.* **2016,** *55* (29), 8328-8332.

TOC Graphic

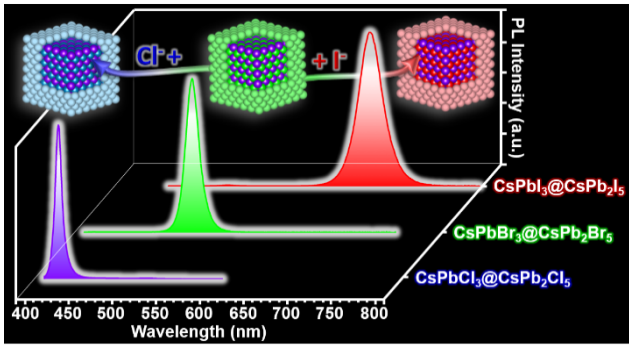
Cl⁻+
+ I⁻
PL Intensity (a.u.)
CsPbI3@CsPb2I5
CsPbBr3@CsPb2Br5
CsPbCl3@CsPb2Cl5
400 450 500 550 600 650 700 750 800
Wavelength (nm)